Synthesis and Characterization of α-, β-, and γ-Ga_2O_3 prepared from Aqueous Solutions by Controlled Precipitation

Liandi Li,[1,2,3] *Wei Wei,*[1] *Malte Behrens*[2,*]

[1] State Key Laboratory of Coal Conversion, Institute of Coal Chemistry, Chinese Academy of Sciences, Taiyuan, 030001, PR China

[2] Fritz-Haber-Institute of Max Planck Society, Department of Inorganic Chemistry, Faradayweg 4-6, 14195 Berlin, Germany

[3] Graduate University of Chinese Academy of Sciences, Beijing, 100049, PR China

* Corresponding author. E-mail: behrens@fhi-berlin.mpg.de, Tel.: +49 30 8413-4408, Fax: +49 30 8413-4405

Abstract

α, β and γ-Ga_2O_3 have been successfully obtained in an easily scalable synthesis using aqueous solution of gallium nitrate and sodium carbonate as starting materials without any surfactant and additive. α and β-Ga_2O_3 were obtained by calcination at 350 and 700 °C, respectively, of α-GaOOH, prepared by controlled precipitation at constant pH 6 and T = 55 °C, with 24 h of aging. Aging was necessary to fully convert the initially preciptated gel into a well-crystalline and phase-pure material. γ-Ga_2O_3 was obtained after calcination at 500 °C of gallia gel, synthesized at constant pH 4 and T = 25 °C, without aging. These three polymorphs have a for gallia relatively high surface area: 55 m^2/g (α-Ga_2O_3), 23 m^2/g (β-Ga_2O_3) and 116 m^2/g (γ-Ga_2O_3). The combination of X-ray diffraction (XRD), scanning electron microscopy (SEM), energy dispersive X-ray analysis (EDX), nitrogen physisoption and thermogravimetry (TG) was employed to characterize the samples and their formation.

Keywords

Gallium, Oxide, Porosity, Polymorphism

1. Introduction

Gallium oxide is widely used for the preparation of gas sensors, optoelectronic devices, luminescent materials and catalysts in diverse gas and liquid phase chemical reactions [1-11]. It is an insulator with a wide band gap at room temperature (~4.9 eV for β-Ga_2O_3) , which is considered to be the widest band gap semiconductor among transparent conducting oxides (TCOs) [12-14]. However, preparation of β-Ga_2O_3 under reducing conditions or heating in reducing atmospheres at high temperature turns it into an n-type semiconductor. [1,6,7,15]. For example, a substantial conductivity increase was observed for β-Ga_2O_3 crystals, when grown under reducing conditions in an inductive couples plasma torch. This increase could be quenched again upon annealing in oxygen, indicating that oxygen vacancies are the source of the enhanced conductivity [16]. Such vacancies act as shallow donors and their role on the luminescence properties of β-Ga_2O_3 has been studied in detail by Binet and Gourier [17]. Gallium oxide is also used as a catalyst support, in particular for Pd-based catalysts. In such systems, the partial reduction of Ga^{III} may lead to the formation of Ga-Pd intermetallic compounds, which have interesting properties in methanol synthesis [18], methanol steam reforming [19-24] and hydrogenation reactions [25,26]. A large specific surface area of nano-structured gallium oxide is desired for both applications as gas sensor and catalyst [2].

Five modifications of Ga_2O_3 are known: α, β, γ, δ and ε [27] and a thermodynamic description of the system Ga-O has been presented [28]. Among these five modifications, β-Ga_2O_3 is the most stable modification (mp 1740 °C); it has a monoclinic structure with the oxide ions in distorted ccp arrangement and Ga^{III} in distorted tetrahedral and octahedral sites [29-31]. α-Ga_2O_3 crystallizes in the structure of corundum. It forms upon heating of α-

GaOOH in air between 450 and 550 °C [28]. It also has been reported by Remeika and Marezio that single crystals of α-Ga_2O_3 have been grown from a flux at a pressure of 44 kbar and at a temperature of 1000 °C [32]. γ-Ga_2O_3 is assumed as a cubic spinel-type structure [33]. Böhm has described the preparation of this gallia polymorph and found a crystal structure similar to that of γ-Al_2O_3 [34]. Zinkevich et al. found differences in the cation distribution between both compounds and discuss the similarity of γ-Ga_2O_3 with η-Al_2O_3 [35]. Areán and Delgado have reported that γ-Ga_2O_3 was prepared by calcination (at 500 °C) of a gallia gel obtained by adding ammonia to an ethanolic solution of gallium nitrate. They attributed the presence of excess water in gallia gels to the formation of a product, probably GaOOH, which is not a precursor of γ-Ga_2O_3 but rather of the α-Ga_2O_3 polymorph. Hence, they advised to avoid the use of water as a solvent when preparing γ-Ga_2O_3 [30,33]. δ-Ga_2O_3 crystallizes like In_2O_3 in the C-type structure of rare earths [28]. It can be prepared by heating the residual of evaporated gallium nitrate solution at 200-250 °C. When it is heated above 500 °C, the δ modification transforms to orthorhombic ε-Ga_2O_3 [28]. In summary, the polymorphism of Ga_2O_3 is very similar to that of Al_2O_3: α-, β-, γ- and ε-Ga_2O_3 are isomorphous with α-, θ-, γ- or η- and κ-Al_2O_3, respectively, but there is no form of Al_2O_3 that corresponds to δ-Ga_2O_3 [27].

In the present work, we have investigated a simple aqueous chemistry route to synthesize precursors of Ga_2O_3, and showed that not only α-, β-, but also γ-Ga_2O_3 can be formed by thermal treatment of precursors obtained from aqueous solution. The detailed characterization work, effect of different synthesis parameters like pH and temperature, will be discussed.

2. Experimental Section

2.1. Synthesis Procedures

To prepare the α- and β-Ga_2O_3 polymorphs, their precursor was synthesized by controlled precipitation at constant pH 6 and a temperature of 55 °C using co-feeding of appropriate amounts of 0.1 M gallium nitrate and 0.345 M sodium carbonate solution as precipitating agent to maintain a constant pH. Both solutions were added simultaneously dropwise into a 2 L automated reactor, which was filled prior to the precipitation with bidistilled H_2O (300 mL) [36]. The gallium nitrate solution was automatically pumped with a constant dosing rate (16 mg/min) and the sodium carbonate solution was added to maintain a constant pH. In a typical experiment, the addition of approximately 250 g of the $Ga(NO_3)_3$ solution required dosing of approximately 110 g of the soda solution (Fig, 1, inset). After completion of addition, the precipitates were aged for 24 h at the precipitation temperature under stirring. The whole process was controlled by a computer-controlled automated reactor system (Labmax, Mettler-Toledo) used to control the precipitation process parameters. After filtration, the precipitate was washed two times each with bidistilled water (400 mL). Then, the precipitate was dried at 80 °C in air for 12 h. Finally, the dried samples were calcined at 350 and 700 °C in static air for 2 h to get α- and β-Ga_2O_3, respectively.

To prepare the γ-Ga_2O_3 polymorph, 0.1 M gallium nitrate and 0.345 M sodium carbonate solutions as precipitating agent were added simultaneously dropwise into the 2 L reactor, prefilled with bidistilled H_2O (300 mL). While the dosing rate was unchanged, pH and temperature were lower compared to the preparation of the precursor for the α- and β-phase (pH 4, T = 25 °C). After completion of addition, the precipitate was directly filtered without

aging and washed two times with bidistilled water (400 mL). Then, the precipitate was dried at room temperature (RT) in air for 3 days. Finally, the dried sample was calcined at 500 °C in static air for 2 h to obtain γ-Ga_2O_3.

2.2. Characterization Techniques

The crystalline phases of products were examined by X-ray diffraction (XRD) on a STOE Stadi P diffractometer in transmission geometry using Cu $K\alpha_1$ radiation, a primary Ge monochromater and a 3º linear position sensitive detector. Furthermore, the Rietveld crystal structure refinement of the XRD pattern was carried out using the TOPAS software [37] and crystal structure data were from the ICSD database. The size and morphology of the resulting products were observed by Scanning Electron Microscope (SEM) at an acceleration voltage of 2.0 kV. Energy Dispersed X-ray Spectroscopy (EDX) was performed on the same SEM. The specific surface area was determined by nitrogen physisoption in an Autosorb-1C setup (Quantachrome) using the Brunauer-Emmett-Teller (BET) method based on nitrogen adsorption-desorption. Thermogravimetry (TG) was performed on a Netzsch STA449 thermobalance (2 °C / min, synthetic air). Temperature programmed reduction (TPR) was done in a fixed bed reactor (TPDRO-1100, CE instruments) with a 5 % H_2 in He gas (80 ml/min) at a heating rate of 2 K/min. The H_2 consumption was monitored with a thermal conductivity detector.

3. Results and Discussion

3.1. α-GaOOH Precursor

To generate Ga_2O_3 of homogeneous microstructure, it is important to first develop a method to fabricate a phase-pure precursor [38]. It has been demonstrated that gallium oxide hydroxide (α-GaOOH), which crystallizes with α-AlOOH structure type (diaspore, Pbnm) undergoes transformation to gallium oxide during thermal treatment [2,39].

The aging time has a great effect on the crystallinity and morphology of precipitate products. Fig. 1 shows the precipitation and aging log for the preparation of the precursor. Precipitation is performed at constant pH by simultaneous dosing of metal solution and precipitating agent ($t_{aging} < 0$ in Fig. 1). The inset in Fig. 1 is a magnification of the range from -0.4 to 0.2 h. After some stronger oscillations at the beginning of precipitation, the pH is kept constant within 1 unit. After precipitation, pH increases to 7 with the 1st hour of aging and then increases linearly to pH 8 after 24 hours. This slow and steady increase does not level off and is not related to continuous changes of the solid in the suspension due to dissolution or re-crystallization events, but rather due to gradual changes in the open system (solvent evaporation, CO_2 emission). An analogous experiment with pure neutralized $NaCO_3$ solution showed the same trend in pH. A steady drift of the pH probe could also cause apparent pH changes at such long measurement times, but was found by calibration experiments to have a negligible contribution for the used setup. The XRD patterns of as-formed products synthesized under pH 6 at 55 °C with 0, 0.5, 1, 3, 6, 12 and 24 h of aging and dried at 80 °C for 12 h are shown in Fig. 2. The intensity of diffraction lines becomes more intense with aging time, suggesting that the crystallinity increases. We conclude that during precipitation, at first an amorphous material or a precipitate with very small crystallites is formed, which is transformed into the well crystalline precursor after aging in the mother liquor for 24 h. The intermediate presence of two types of material can be corroborated by the SEM images (Fig.

3) of precipitates taken after different aging time. In Fig. 3a, it is found that the sample with 1 h of aging is comprised of aggregates of elongated platelet-like particles forming a spindle- or rice grain-like shape together with a lot of material of ill-defined morphology exhibiting much lower particle sizes (see arrows). From the trend seen in XRD (Fig. 2), it is assumed that the material with the small particle size is representative of the amorphous initial precipitation product that dominates the XRD patterns at low aging times. A spindle-like morphology has also been reported by Tas et al. for crystalline GaOOH precipitates [1]. The platelet-like primary particles exhibit an average length of 100 ~ 1200 nm, a width of 80 ~ 150 nm, and a thickness of 5 ~ 20 nm. After 12 h aging time, the maximal detected length and width has increased to 1500 nm and 200 nm, respectively. The other type of material, which is presumed to be less-crystalline, is still clearly detectable (Fig. 3b). After longer aging time, 24 h, the platelet-like particles have maintained their size and the smaller particles at their surface have disappeared indicating that under the conditions chosen a prolonged aging time is necessary to fully crystallize the precipitate (Fig. 3c). The necessity of a long aging period for complete crystallization of GaOOH from the initially amorphous precipitate has been previously reported by Sato and Nakamura [40]. It is noted that in our experiment the elongated crystallization period and its effect on the material's homogeneity cannot be easily seen in the XRD data alone, which exhibits only very subtle changes after an aging period of ca. 3 h (Fig. 2).

By XRD the sample obtained after 24 h of aging can be identified as pure gallium oxide hydroxide, α-GaOOH (orthorhombic, Pnma). A Rietveld plot is shown in Fig. 4a. The experimental lattice parameters are a = 9.8089(2) Å, b = 2.9742(1) Å, c = 4.5710(2) Å, slightly larger than those reported by Li et al. [41] (a = 9.7907(8) Å, b = 2.9732(2) Å, c =

4.5171(4) Å). The chemical composition of this sample was investigated with EDX, which indicates an atomic ratio between O and Ga of 2.55, different from O: Ga = 2 expected for α-GaOOH. This oxygen excess is also reflected in the TG-MS curve (Fig. 5a). The total weight loss of our sample is 13.7%, higher than the theoretical weight loss for the conversion of α-GaOOH to Ga_2O_3 of 8.8%. In the light of the low drying temperature and in agreement with literature reports [1,42], it is suggested that the deviation from the theoretical weight loss might be attributed to the release of physically surface adsorbed water, surface bound hydroxyl groups and water inclusions in the crystal lattice, which may also serve as an explanation for the enlarged lattice parameters of our sample.

In conclusion, the effect of increased aging time in the synthesis of α-GaOOH is to give a well crystalline sample. α-GaOOH synthesized at pH 6 and 55 °C after 24 h of aging time is phase pure, which is confirmed by the combination of XRD and SEM. After mild drying at 80 °C, the material still contains a considerable amount of humidity.

3.2. α- and β-Ga_2O_3 Formation

The XRD patterns of the α-GaOOH precursor, after treatment at different calcination temperatures, are shown in Fig. 6. α-GaOOH is still the only phase after calcination at 300 °C for 2 h, which is in agreement with the observation that α-GaOOH is stable up to 300 °C [1,28,31,38] (Fig. 4a). The lattice constants have slightly decreased compared to the dried precursor (a = 9.7885(2) Å, b = 2.9730(1) Å, c = 4.5197(2) Å) (Rietveld plot is shown in Fig. 4b) supporting the idea that crystal water removal occurs as the first step of calcination. The XRD pattern of the sample after calcination at 350 °C for 2 h is different and can be identified as the rhombohedral phase of gallia, α-Ga_2O_3 ($R\bar{3}c$). The Rietveld plot is shown in

Fig. 4c and the experimentally determined lattice parameters are a = 4.9873(3) Å and c = 13.450(1) Å, which is in good agreement with literature values (a = 4.9825(5) Å, c = 13.433(1) Å [43]). When the calcination temperature exceeds 700 °C, the material is transformed to the monoclinic polymorph (C2/m) of gallia, β-Ga_2O_3. The experimental lattice parameters are a = 12.288(1) Å, b = 3.0364(3) Å, c = 5.8085(5) Å, β = 103.78(1) º and similar to the previously reported values of a = 12.214(3) Å, b = 3.0371(9) Å, c = 5.7981(9) Å, β = 103.83(2) º [44]. A graphical representationof the the Rietveld fit is shown in Fig. 4d.

The calcination behavior of α-GaOOH can be also followed by SEM micrographs shown in Fig. 7. Fig. 7a through d show the surface morphology of spindle-like particles after calcination for 2 h in air at 350, 650, 700 and 950 °C, respectively. The initial shape and size of the aggregates are basically conserved during the phase transformation from α-GaOOH to α-Ga_2O_3 and then to β-Ga_2O_3, but the platelet-like shape of the primary particle gradually fades as the calcination temperature is increased. In addition, nano-sized pores appear on their surfaces and are enlarged as calcination temperature is increased. Table 1 summarizes textural properties of the gallium oxide hydroxide and gallium oxides obtained after calcination. The adsorption-desorption isotherm of nitrogen and pore size distribution curve are shown in Fig. 8. All isotherms are typical for mesoporous materials containing micropores [45]. The fact that the hysteresis loop moves to a higher relative pressure as the calcination temperature increases suggests that the most frequent pores are wider for β-Ga_2O_3 than for α-Ga_2O_3 [46]. The pore size distribution was analyzed following the BJH method applied to the desorption branch of the isotherm. In most cases, a very narrow maximum at d = 4 nm is observed. Such sharp signal was not found in the pore size distribution derived from the adsorption branch, which is exemplified in Figure 8f. Thus, the maximum at 4 nm is

not reflecting the porous properties of the material, but rather identified as the so-called tensile strength effect phenomenon, an artifact due to the forced closure of the hysteresis loop with a sudden drop of the isotherm along the desorption branch in the p/p^o range 0.41-0.48, which was described in detail by Groen et al. [47]. For this study, desorption data is used for the particle size distribution, which is considered more accurate compared to adsorption data, and the signal at d = 4 nm is ignored in the analysis. Thus, the real pore size distributions of the Gallia materials show a broader maximum at pore diameters between 3 and 18 nm (Fig. 8, insets). While the loss of surface area with higher calcination temperature (with the exception of the transformation to β-Ga_2O_3, Table 1) suggests considerable sintering and particle growth, we cannot find growth and coalescence of particles in the SEM images (Fig. 7). Thus, these phenomenons could be explained by the decreasing number and widening of the original pores inside the original aggregates, which gives rise to a shift of the broad peak in the pore size distribution with calcinations temperature from 5 to 18 nm (Fig. 8a-d, insets). Tas et al. reported that in a loose powder compact the crystals fused together at their mutual point of contact after calcination at 1200 °C for 6 h [1].

Summarizing this part, treatment at relatively low temperature results in α-Ga_2O_3 with relatively high surface area of 55 m^2g^{-1} and pores of a diameter of ca. 10 nm. As the calcination temperature is increased, the pores widen and specific surface area decreases without significant change of the aggregate sizes. A similar behavior is observed for β-Ga_2O_3, which can be obtained with 23 m^2g^{-1} and 25 nm-pores. Thus, phase-pure α- and β-Ga_2O_3 with relatively large surface area and high pore volume can be produced by calcination of α-GaOOH at 350 and 700 °C in air for 2 h, respectively.

3.3. γ-Ga_2O_3 Formation

When preparing the precursor material, crystal growth and crystal morphology in the precipitation suspension are governed by many factors, for example, the degree of supersaturation, the diffusion of the reactant, the species at the surface of the crystals, the surface and interfacial energies, and the structure of the crystals [48,49].

Previous studies showed that the fresh precipitates exist as gallium hydroxide $Ga(OH)_3$, the precursor of γ-Ga_2O_3 [33,37,40], which probably is seen in the SEM images of the incompletely crystallized samples at aging time of less than 24 h (Fig. 3a,b, arrows). Acidity during precipitation and aging is an important factor to influence olation and the degree of oxolation in the hydroxide precipate, resulting in partial morphological and dimensional control particularly for low dimensional nanocrystals [37,49,50-52]. Crystallinity and morphology of α-GaOOH are sensitive to pH and the type of alkali [1,49]. In alkaline aqueous solutions there is a relatively fast transformation of $Ga(OH)_3$ gel even at room temperature involving oxolation and condensation to α-GaOOH, which is the precursor of α-Ga_2O_3 [31,37,40] (see above). Additionally, contact of the precipitate with base plays a role for recovery of the precursor of γ-Ga_2O_3, because it could promote oxolation.

In order to suppress oxolation and to slow down the transformation from $Ga(OH)_3$ to α-GaOOH, during our experiment, we lowered the pH and temperature of precipitation to pH 4 and 25 °C and filtered the precipitate quickly after synthesis without aging. The XRD pattern of this precipitate (dried at RT for 3 days, Fig. 9a), exhibits only broad diffraction maxima without sharp peaks, indicating that this sample is composed of an amorphous phase or of very small crystallites. This is in agreement with its high surface area (Table 1). Regarding

the morphology, no well developed facets of the particles could be seen in the SEM image (Fig. 10a).

It is noted that when the same synthesis was done at a slightly higher pH of 4.9, faceted particles, most likely the α-GaOOH phase, could be detected by scanning transmission electron microscopy (STEM, encircled areas in Fig. 10f). This type of material could not be detected in XRD (not shown) or normal SEM (Fig. 10e) probably due to its low amount in the sample mixture. For a synthesis pH of 4, however, no such faceted areas could be observed in STEM (Fig. 10b) indicating that a low pH helps to hinder the crystallization of the $Ga(OH)_3$ precursor gel in aqueous suspensions.

The chemical composition of the homogenous sample obtained at pH 4 was investigated with EDX. It shows an average atomic ratio between O and Ga of approximately 1.5. The thermogravimetry (TG) and differential thermal analysis (DTA) of this material are shown in Fig. 5b. According to the thermal decomposition of $Ga(OH)_3$ ($2\ Ga(OH)_3 \rightarrow Ga_2O_3 + 3\ H_2O$), the theoretical mass loss 22.4%, exceeding only moderately the experimental mass loss of 18.9%. This corresponds to an atomic ratio between O and Ga of 2.7, in strong deviation from the EDX result and close to the expected value of 3. This difference can be explained with the tendency of $Ga(OH)_3$ to easily dehydrate in the electron beam and in the vacuum of the SEM chamber to form partially dehydrated gallia [28]. Thus, the EDX results are considered unreliable and the precursor should be a gel of a composition near $Ga(OH)_3$.

TG analysis shows that the dehydration is not complete before approximately ca. 400 °C (Fig. 5b). It has been reported that γ-Ga_2O_3 can reactively adsorb up to 0.6 moles of H_2O [35]. While the endothermic signal at 69 °C in DTA curve assigned to desorption of adsorbed

water, the weak exothermic peak positioned at 703 °C can be attributed to the transformation to β-Ga_2O_3 (confirmed by XRD, not shown). An increase in the heating rate from 2 to 10 °C/min leads to a clearer exothermic signal (Fig. 5b, dotted line), but also to a significant shift of the peak temperature by 27 °C to higher values. Thus, between ca. 400 and 703 °C, another fully dehydrated phase of Ga_2O_3, different from the β-Ga_2O_3, should be stable. The XRD pattern of the sample after calcination at 500 °C for 2 h exhibits a low crystallinity (Fig. 9b), consistent with its still relatively high surface area (Table 1). It has been reported [30,33,35, 53,54], that the diffractogram of γ-Ga_2O_3 closely resembles that of γ- and η-alumina with the exception of a shift towards lower Bragg angles, as expected for the larger Ga^{3+} ions. No strong morphological change due to calcination could be detected by SEM or STEM (Fig. 10c, d). The microstructure of γ-Ga_2O_3 has been studied by transmission electron microscopy (TEM) and aggregates of small nano-crystals with the spinel structure have been observed [35]. In summary, the above results provide strong indications that the preparation method used yields γ-Ga_2O_3.

The adsorption-desorption isotherm of nitrogen and pore size distribution curve are shown in Fig. 8e and f. The isotherm shape of the gel precursor and γ-Ga_2O_3 is typical of a mesoporous material. However, the hysteresis loop extending to the lowest attainable pressures suggests that the samples contain micropores [45]. Analysis of the pore size distribution of the gel following the BJH method does not result in a peak > 1.5 nm and suggests that micropores are dominant in this material. Regarding γ-Ga_2O_3, a maximum in the pore size distribution is found at 3 nm (Fig. 8f, inset).

The reducibility of γ-Ga_2O_3 was studied by H_2-TPR and the results are shown in Fig. 11. It has been reported that pure gallium oxide cannot be reduced by hydrogen below 627 °C. Only when β-Ga_2O_3 is contacted with zeolite, it is amenable to reduction by H_2 [55,56]. Accordingly, the TPR profiles of the well-crystalline α- and β-Ga_2O_3, which are shown in Fig. 11 for comparison, do not show any signal of hydrogen consumption during the heating experiment up to 600 °C (Fig. 11a,b). The highly dispersed and poorly crystalline γ-Ga_2O_3, however, exhibits a clear reduction peak at 344 °C. Surface reduction by oxygen abstraction in gallium oxide has been reported to be possible already at relatively low temperatures [6,7]. The degree of Ga^{3+} reduction was estimated from the hydrogen consumption assuming Ga^{+} as the formed species. The results suggest that less than 2 % of the Ga^{3+}-ions in the sample have been reduced. Thus, we assign the TPR peak to the surface reduction of γ-Ga_2O_3 and ascribe its high reactivity to the lack of structural order and the relatively high intensity of the signal to the large specific surface area of the γ-Ga_2O_3 sample.

4. Conclusions

A scheme similar to that presented in ref [27] summarizes the results of this study and is shown in Fig. 12. Assuming amorphous $Ga(OH)_3$ gel as the initial production of precipitation, two different pathways can be followed using an aqueous solution of gallium nitrate and sodium carbonate as precipitating agent. At high pH and T, the precipitate readily dehydrates to form crystalline α-GaOOH. At pH 6 and 55 °C, the complete crystallization requires an aging period of 24 h and yields aggregated particles of spindle-like morphology. Thermal treatment of this material allows some control over the porosity of the α- and β-Ga_2O_3 materials formed at calcination temperature above 350 and 700 °C, respectively. If the

precipitation is done at lower pH and T without aging, an amorphous and microporous $Ga(OH)_3$ gel can be stabilized. By calcination at 500 °C, γ-Ga_2O_3 with high surface area of 116 m^2g^{-1} can be obtained. Near 700 °C, the γ-phase transforms into the stable β-phase. This synthesis scheme of Gallia will be used in further studies for the preparation of noble metal catalysts supported on difference polymorphs of Gallia by co-precipitation.

Acknowledgements

G. Weinberg, G. Lorenz, F. Girgsdies and E. Kitzelmann (FHI-AC, Berlin) are acknowledged for their help with various sample characterizations. R. Schlögl is acknowledged for his support and fruitful discussions. The doctoral student exchange program of the Chinese Academy of Science and the Max Planck Society has provided financial support.

Figure Captions:

Fig. 1. Evolution of pH during precipitation and aging of α-GaOOH precursor.

Fig. 2. a. XRD pattern of samples obtained from controlled precipitation of $Ga(NO_3)_3$ by Na_2CO_3 at pH 6 and 55 °C with different aging time, and then dried at 80 °C for 12 h;

Fig. 3. SEM images of the samples obtained after (b, c) 1 h, (d, e) 12 h and (f, g) 24 h of aging time (arrows mark the small particle clusters at the surface of the larger aggregates).

Fig. 4. Rietveld refinements of the samples synthesized at pH 6 and 55 °C after 24 h of aging, (a), then calcined at (b) 300, (c) 350 and (d) 700 °C, in air for 2 h (data point are experimental data, the black line is calculated pattern and the grey line is the difference between experiment and fit, and tick marks refer to positions of Bragg reflections); crystal structures of α-GaOOH (e), α-Ga_2O_3 (f) and β-Ga_2O_3 (g) (white balls represent H^+ ions, black balls represent O^{2-} ions, and Ga^{3+} ions occupy interstices within the lattice of O^{2-} ions).

Fig. 5. a. TGA-MS for α-GaOOH. The black line is the TG curve, and the grey line is the ion current of m/e = 18 (H_2O); b. TGA-DTA of $Ga(OH)_3$ gel.

Fig. 6. XRD patterns of samples synthesized by controlled precipitation at pH 6 and 55 °C with 24 h of aging, and dried at 80 °C for 12 h, then calcinated at varying temperatures.

Fig. 7. SEM images showing the morphology of samples synthesized at pH 6 and 55 °C after 24 h of aging, and dried at 80 °C for 12 h, then calcinated at (a, b) 350, (c, d) 650, (e, f) 700 and (g, h) 950 °C, in air for 2 h.

Fig. 8. N_2 adsorption-desorption isotherms and BJH pore size distribution (insets): α-Ga_2O_3 with different calcination temperature a. 350 °C, b. 650 °C; β-Ga_2O_3 with different calcination temperature c. 700 °C, d. 950 °C; e. $Ga(OH)_3$ gel; f. γ-Ga_2O_3 calcinated at 500 °C. In the inset in f) also the pore size distribution derived from the adsorption branch is shown. The sharp signal observed around 4 nm is identified as an artifact by comparison with the adsorption data.

Fig. 9. a. XRD pattern of sample synthesized under pH 4 at 25 °C without aging and dried at RT for 3 days; b. XRD pattern of sample (a) calcinated at 500 °C in air for 2 h (the histogram represents γ-Ga_2O_3 with ICSD Nr. 152085).

Fig. 10. a. SEM image showing the morphology of sample synthesized at pH 4 and 25 °C without aging, after dried at RT for 3 days, with its STEM image (b); c. then calcinated at 500 °C in air for 2 h, and d is the corresponding STEM image. e. SEM image showing the morphology of sample synthesized at pH 4.9 and 25 °C without aging, after dried at 80 °C for 12 h, with its STEM image (f).

Fig. 11. TPR profiles of the α (a), β (b) and γ (c) -Ga_2O_3.

Fig. 12. Schematic illustration showing the synthesis of α, β, γ-Ga_2O_3 by controlled precipitation and thermal treatment.

Table 1: Textural properties of gallium oxides and their precursors.

Sample[a]	**FHI database number**[b]	**Surface area (m^2/g)**	**Pore diameter (nm)**	**Pore volume (cm^3/g)**
α-GaOOH	9111	5	19.2	$1.9*10^{-2}$
α-Ga_2O_3 (350)	9125	55	10.1	$1.4*10^{-1}$
α-Ga_2O_3 (650)	9171	17	30.0	$1.2*10^{-1}$
β-Ga_2O_3 (700)	9172	23	25.2	$1.5*10^{-1}$
β-Ga_2O_3 (950)	9196	16	35.8	$1.4*10^{-1}$
$Ga(OH)_3$ gel	10459	207	2.6	$1.3*10^{-1}$
γ-Ga_2O_3 (500)	10846	116	6.6	$1.9*10^{-1}$

[a] Numbers in parentheses give the calcination temperature in °C

[b] To facilitate sample identification and communication, please refer to these labels upon correspondence.

References

[1] A. C. Tas, P. J. Majewski, F. Aldinger, J. Am. Ceram. Soc. 85 (2002) 1421-1429.

[2] Y. Zhao, R. L. Frost, J. Yang, W. N. Martens, J. Phys. Chem. C 112 (2008) 3568-3579.

[3] C. A. Deshmane, J. B. Jasinski, M. A. Carreon, Microporous Mesoporous Mater. 130 (2010) 97-102.

[4] M. Ogita, N. Saika, Y. Nakanishi, Y. Hatanaka, Appl. Surf. Sci. 142 (1999) 188-191.

[5] T. Weh, J. Frank, M. Fleischer, H. Meixner, Sens. Actuators B: Chem. 78 (2001) 202-207.

[6] W. Jochum, S. Penner, R. Kramer, K. Föttinger, G. Rupprechter, B. Klötzer, J. Catal. 256 (2008) 268-277.

[7] W. Jochum, S. Penner, R. Kramer, K. Föttinger, G. Rupprechter, B. Klötzer, J. Catal. 256 (2008) 278-286.

[8] K. Nakagawa, C. Kajita, Y. Die, M. Okamura, S. Kato, H. Kasuya, N. Ikenaga, T. Kobayashi, T. Suzuki, Catal. Lett. 64 (2000) 215-221.

[9] K. Shimizu, A. Satsuma, T. Hattori, Appl. Catal. B 16 (1998) 319-326.

[10] P. P. Pescarmona, K. P. F. Janssen, P. A. Jacobs, Chem. Eur. J. 13 (2007) 6562-6572.

[11] P. P. Pescarmona, P. A. Jacobs, Catal. Today 137 (2008) 52-60.

[12] S. Sharma, M. K. Sunkara, J. Am. Chem. Soc. 124 (2002) 12288-12293.

[13] L. Binet, D. Gourier, C. Minot, J. Solid State Chem. 113 (1994) 420-433.

[14] Y. Zhao, R. L. Frost, W. N. Martens, J. Phys. Chem. C 111 (2007) 16290-16299.

[15] T. Wang, S. S. Farvid, M. Abulikemu, P. V. Radovanovic, J. Am. Chem. Soc. 132 (2010) 9250-9252.

[16] M. R. Lorenz, J. F. Woods, R. J. Gambino, J. Phys.Chem.Solids 28 (1967) 403-404.

[17] L. Binet, D. Gourier, J. Phys. Chem. Solids 59 (1998) 1241-1249.

[18] N. Iwasa, H. Suzuki, M. Terashita, M. Arai, N. Takezawa, Catal. Lett. 96 (2004) 75-78.

[19] N. Iwasa, T. Mayanagi, W. Nomura, M. Aral, N. Takezawa, Appl. Catal. A 248 (2003) 153-160.

[20] N. Iwasa, N. Takezawa, Top. Catal. 22 (2003) 215-224.

[21] N. Iwasa, T. Mayanagi, N. Ogawa, K. Sakata, N. Takezawa, Catal. Lett. 54 (1998) 119-123.

[22] S. Penner, H. Lorenz, W. Jochum, M. Stöger-Pollach, D. Wang., C. Rameshan, B. Klötzer, Appl. Catal. A 358 (2009) 193-202.

[23] S. Penner, W. Jochum, C. Rameshan, B. Klötzer, Appl. Catal. A 358 (2009) 203-210.

[24] A. Haghofer, K. Föttinger, F. Girgsdies, D. Teschner, A. Knop-Gericke, R. Schlögl, G. Rupprechter, J. Catal., submitted.

[25] A. Ota, M. Armbrüster, M. Behrens, D. Rosenthal, M. Friedrich, I. Kasatkin, F. Girgsdies, W. Zhang, R. Wagner, R. Schlögl, J. Phys. Chem. C 115 (2011) 1368-1374.

[26] M. Armbrüster, K. Kovnir, M. Behrens, D. Teschner, Y. Grin, R. Schlögl, J. Am. Chem. Soc. 132 (2010) 14745-14747.

[27] M. Zinkevich, F. Aldinger, J. Am. Ceram. Soc. 87 (2004) 683-691.

[28] R. Roy, V. G. Hill, E. F. Osborn, J. Am. Chem. Soc. 74 (1952) 719-722.

[29] N. N. Greenwood, A. Earnshaw, Chemistry of the Elements, 2nd Edition, Elsevier Science Ltd, Burlington, 1997.

[30] M. R. Delgado, C. O. Areán, Z. Anorg. Allg. Chem. 631 (2005) 2115-2120.

[31] A. W. Laubengayer, H. R. Engle, J. Am. Chem. Soc. 61 (1939) 1210-1214.

[32] J. P. Remeika, M. Marezio, Appl. Phys. Lett. 8 (1966) 87-88.

[33] C. O. Areán, A. L. Bellan, M. P. Mentruit, M. R. Delgado, G. T. Palomino, Microporous Mesoporous Mater. 40 (2000) 35-42.

[34] J. Böhm, Angew. Chem. 53 (1940) 131.

[35] M. Zinkevich, F. M: Morales, H. Nitsche, M. Ahrens, M. Rühle, F. Aldinger, Z. Metallk, 95 (2004) 756.

[36] B. Bems, M. Schur, A. Dassenoy, H. Junkes, D. Herein, R. Schlögl, Chem. Eur. J. 9 (2003) 2039-2052.

[37] TOPAS version 4.2, copyright 1999, 2009, Bruker AXS.

[38] H. Qian, P. Gunawan, Y. Zhang, G. Lin, J. Zheng, R. Xu, Cryst. Growth Des. 8 (2008) 1282-1287.

[39] N. A. Nikolaev, L. M. Lityagina, T. I. Dyuzheva, L. F. Kulikova, N. A. Bendeliani, J. Alloys Compd. 459 (2008) 95-97.

[40] T. Sato, T. Nakamura, J. Chem. Technol. Biotechnol. 32 (1982) 469-475.

[41] S. J. Li, C. Zheng, K. C. Lobring, Z. Kristallogr. NCS 218 (2003) 11-12.

[42] X. Liu, G. Qiu, Y. Zhao, N. Zhang, R. Yi, J. Alloys Compd. 439 (2007) 275-278.

[43] M. Marezio, J. P. Remeika, J. Chem. Phys. 46 (1967) 1862-1865.

[44] J. Åhman, G. Svensson, J. Albertsson, Acta Crystallogr., Sect. C: Cryst. Struct. Commun. 52 (1996) 1336-1338.

[45] K. S. W. Sing, D. H. Everett, R. A. W. Haul, L. Moscou, R. A. Pierotti, J. Rouquérol, T. Siemieniewska, Pure Appl. Chem. 57 (1985) 603-619.

[46] M. R. Delgado, D. O. Areán, Mater. Lett. 57 (2003) 2292-2297.

[47] J. Groen, L. A. Peffer, J. Pérez-Ramírez, Microporous Mesoporous Mater. 60 (2003) 1-17.

[48] Q. Tang, W. Zhou, W. Zhang, S. Ou, K. Jiang, W. Yu, Y. Qian, Cryst. Growth Des. 5 (2005) 147-150.

[49] J. Yang, C. Lin, Z. Wang, J. Lin, Inorg. Chem. 45 (2006) 8973-8979.

[50] T. Kawano, H. Imai, Cryst. Growth Des. 6 (2006) 1054-1056.

[51] Y. Tak, K. Yong, J. Phys. Chem. B 109 (2005) 19263-19269.

[52] Y. Chang, H. C. Zeng, Cryst. Growth Des. 4 (2004) 397-402.

[53] B. Zheng, W. Hua, Y. Yue, Z. Gao, J. Catal. 232 (2005) 143-151.

[54] Y. Hou, L. Wu, X. Wang, Z. Ding, Z. Li, X. Fu, J. Catal. 250 (2007) 12-18.

[55] M. Saito, S. Watanabe, I. Takahara, M. Inaba, K. Murata, Catal. Lett. 89 (2003) 213-217.

[56] B. Sulikowski, Z. Olejniczak, V. Cortés Corberán, J. Phys. Chem. 100 (1996) 10323-10330.

Figure Captions:

Fig. 1. Evolution of pH during precipitation and aging of α-GaOOH precursor.

Fig. 2. a. XRD pattern of samples obtained from controlled precipitation of $Ga(NO_3)_3$ by Na_2CO_3 at pH 6 and 55 °C with different aging time, and then dried at 80 °C for 12 h;

Fig. 3. SEM images of the samples obtained after (b, c) 1 h, (d, e) 12 h and (f, g) 24 h of aging time (arrows mark the small particle clusters at the surface of the larger aggregates).

Fig. 4. Rietveld refinements of the samples synthesized at pH 6 and 55 °C after 24 h of aging, (a), then calcined at (b) 300, (c) 350 and (d) 700 °C, in air for 2 h; structural models of α-GaOOH (e), α-Ga_2O_3 (f) and β-Ga_2O_3 (g) (white balls represent H^+ ions, black balls represent O^{2-} ions, and Ga^{3+} ions occupy interstices within the lattice of O^{2-} ions).

Fig. 5. a. TGA-MS for α-GaOOH. The black line is the TG curve, and the grey line is the ion current of m/e = 18 (H_2O); b. TGA-DTA of $Ga(OH)_3$ gel.

Fig. 6. XRD patterns of samples synthesized by controlled precipitation at pH 6 and 55 °C with 24 h of aging, and dried at 80 °C for 12 h, then calcinated at varying temperatures.

Fig. 7. SEM images showing the morphology of samples synthesized at pH 6 and 55 °C after 24 h of aging, and dried at 80 °C for 12 h, then calcinated at (a, b) 350, (c, d) 650, (e, f) 700 and (g, h) 950 °C, in air for 2 h.

Fig. 8. N_2 adsorption-desorption isotherms and BJH pore size distribution (insets): α-Ga_2O_3 with different calcination temperature a. 350 °C, b. 650 °C; β-Ga_2O_3 with different calcination temperature c. 700 °C, d. 950 °C; e. $Ga(OH)_3$ gel; f. γ-Ga_2O_3 calcinated at 500 °C.

In the inset in f) also the pore size distribution derived from the adsorption branch is shown. The sharp signal observed around 4 nm is identified as an artifact by comparison with the adsorption data.

Fig. 9. a. XRD pattern of sample synthesized under pH 4 at 25 °C without aging and dried at RT for 3 days; b. XRD pattern of sample (a) calcinated at 500 °C in air for 2 h (the histogram represents γ-Ga_2O_3 with ICSD Nr. 152085).

Fig. 10. a. SEM image showing the morphology of sample synthesized at pH 4 and 25 °C without aging, after dried at RT for 3 days, with its STEM image (b); c. then calcinated at 500 °C in air for 2 h, and d is the corresponding STEM image. e. SEM image showing the morphology of sample synthesized at pH 4.9 and 25 °C without aging, after dried at 80 °C for 12 h, with its STEM image (f).

Fig. 11. TPR profiles of the α (a), β (b) and γ (c) -Ga_2O_3.

Fig. 12. Schematic illustration showing the synthesis of α, β, γ-Ga_2O_3 by controlled precipitation and thermal treatment.

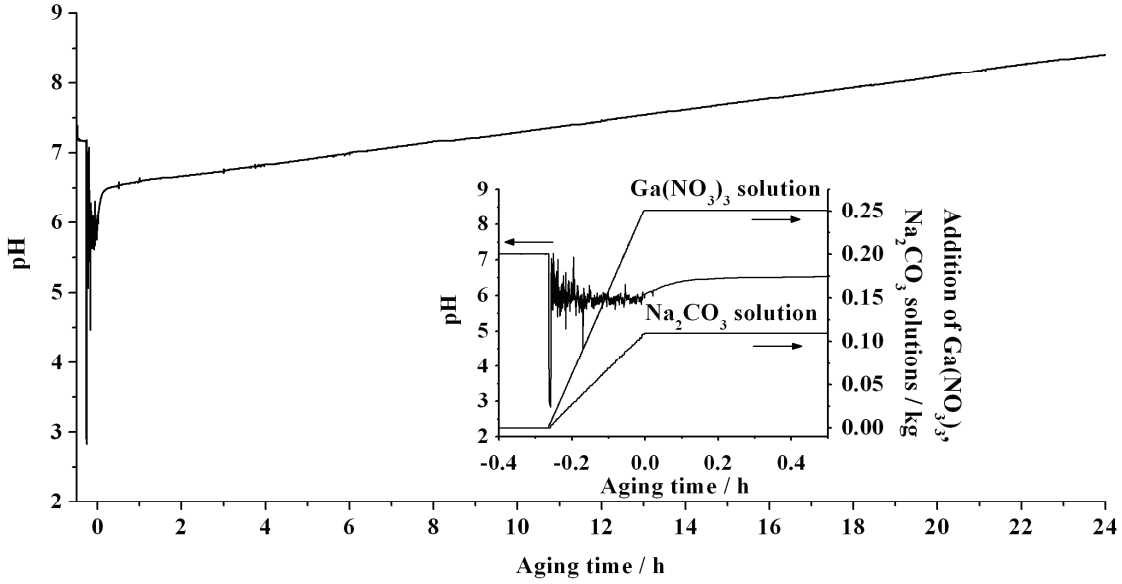
pH
Aging time / h
Ga(NO3)3 solution
Na2CO3 solution
Addition of Ga(NO3)3, Na2CO3 solutions / kg

Figure 1

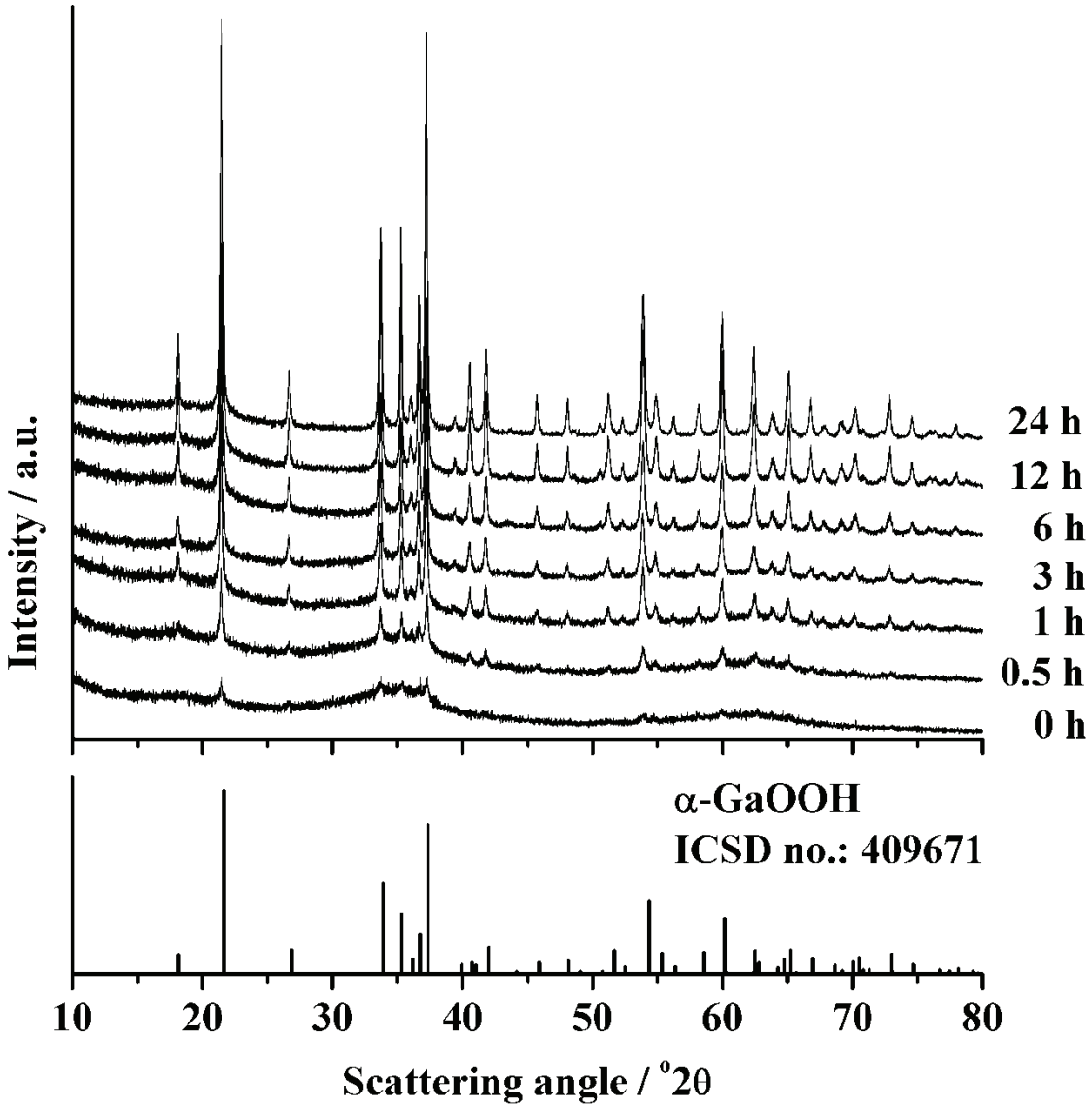
Intensity / a.u.
24 h
12 h
6 h
3 h
1 h
0.5 h
0 h
α-GaOOH
ICSD no.: 409671
10
20
30
40
50
60
70
80
Scattering angle / °2θ

Figure 2

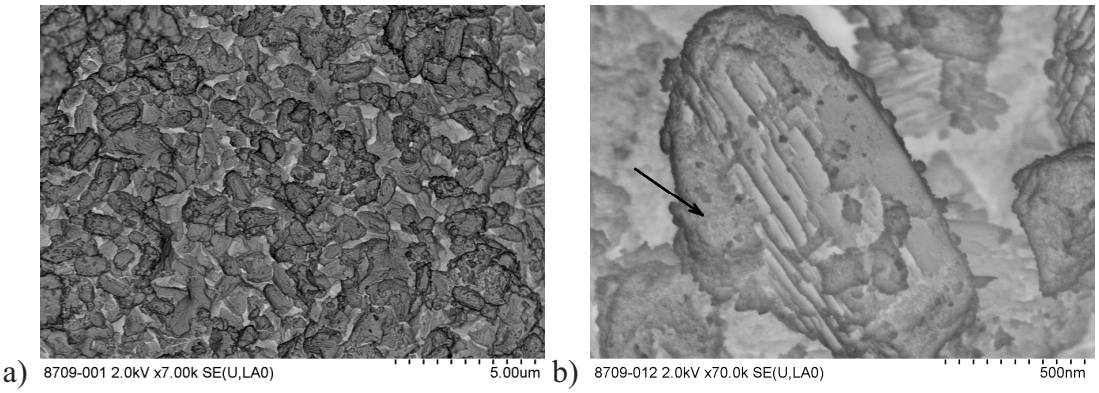
a)
8709-001 2.0kV x7.00k SE(U,LA0)
5.00um
b)
8709-012 2.0kV x70.0k SE(U,LA0)
500nm
c)
8903-001 2.0kV x7.00k SE(U,LA0)
5.00um
d)
8903-007 2.0kV x70.0k SE(U,LA0)
500nm
e)
8909-001 2.0kV x7.00k SE(U,LA0)
5.00um
f)
8909-004 2.0kV x70.0k SE(U,LA0)
500nm

Figure 3

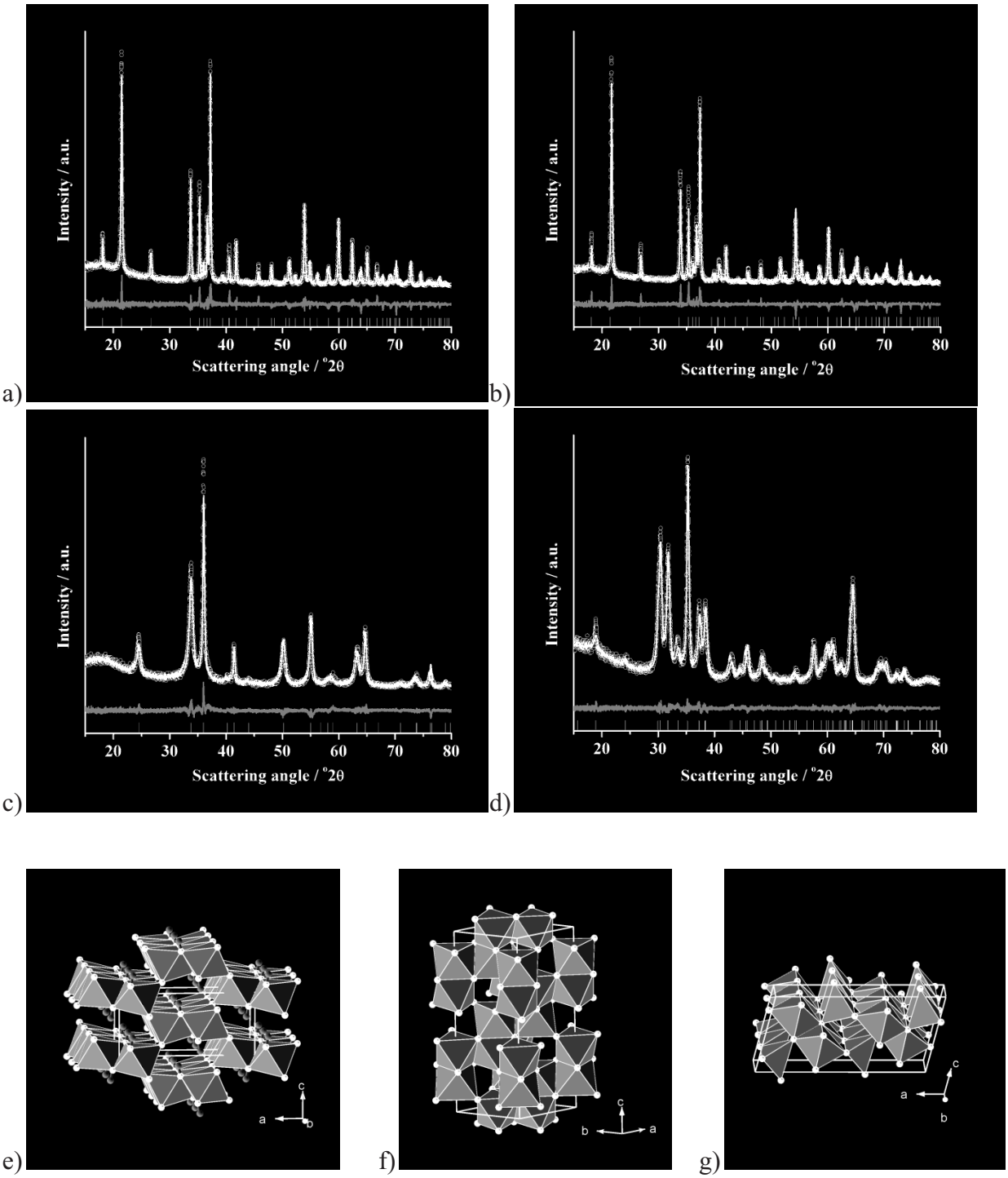
a)
b)
c)
d)
e)
f)
g)
Intensity / a.u.
Scattering angle / °2θ
20
30
40
50
60
70
80
c
a
b

Figure 4

a)

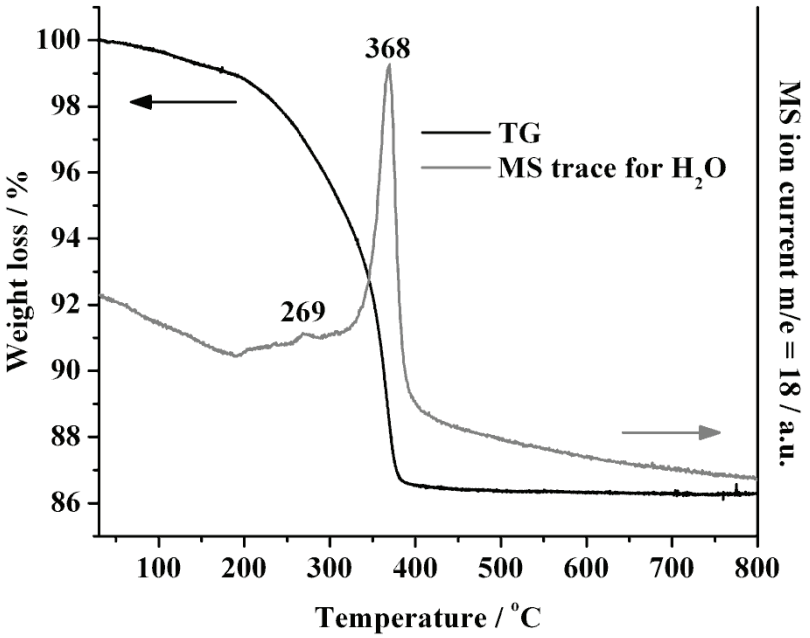
100
98
96
94
92
90
88
86
Weight loss / %
368
269
TG
MS trace for H_2O
MS ion current m/e = 18 / a.u.
100
200
300
400
500
600
700
800
Temperature / °C

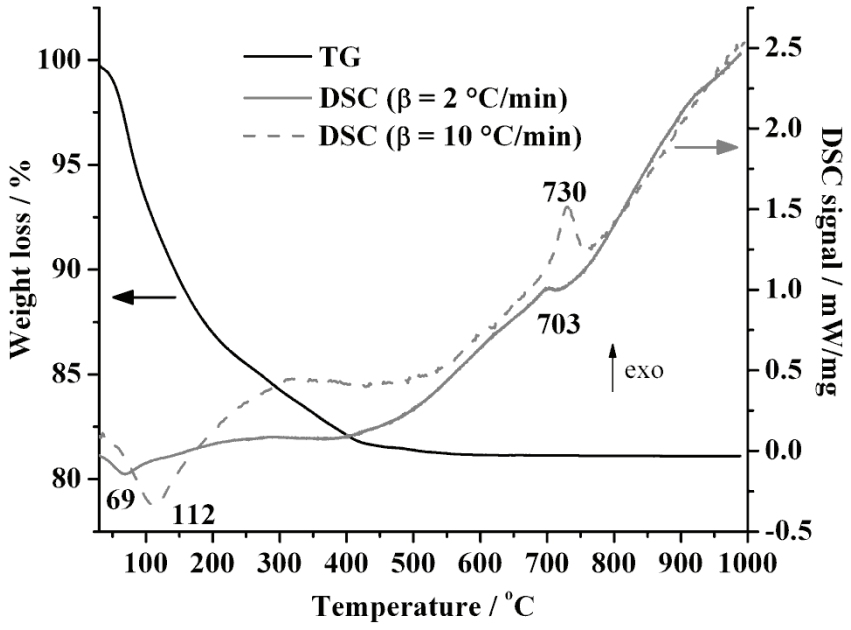
100
95
90
85
80
Weight loss / %
TG
DSC (β = 2 °C/min)
DSC (β = 10 °C/min)
730
703
exo
69
112
2.5
2.0
1.5
1.0
0.5
0.0
-0.5
DSC signal / mW/mg
100
200
300
400
500
600
700
800
900
1000
Temperature / °C

b)

Figure 5

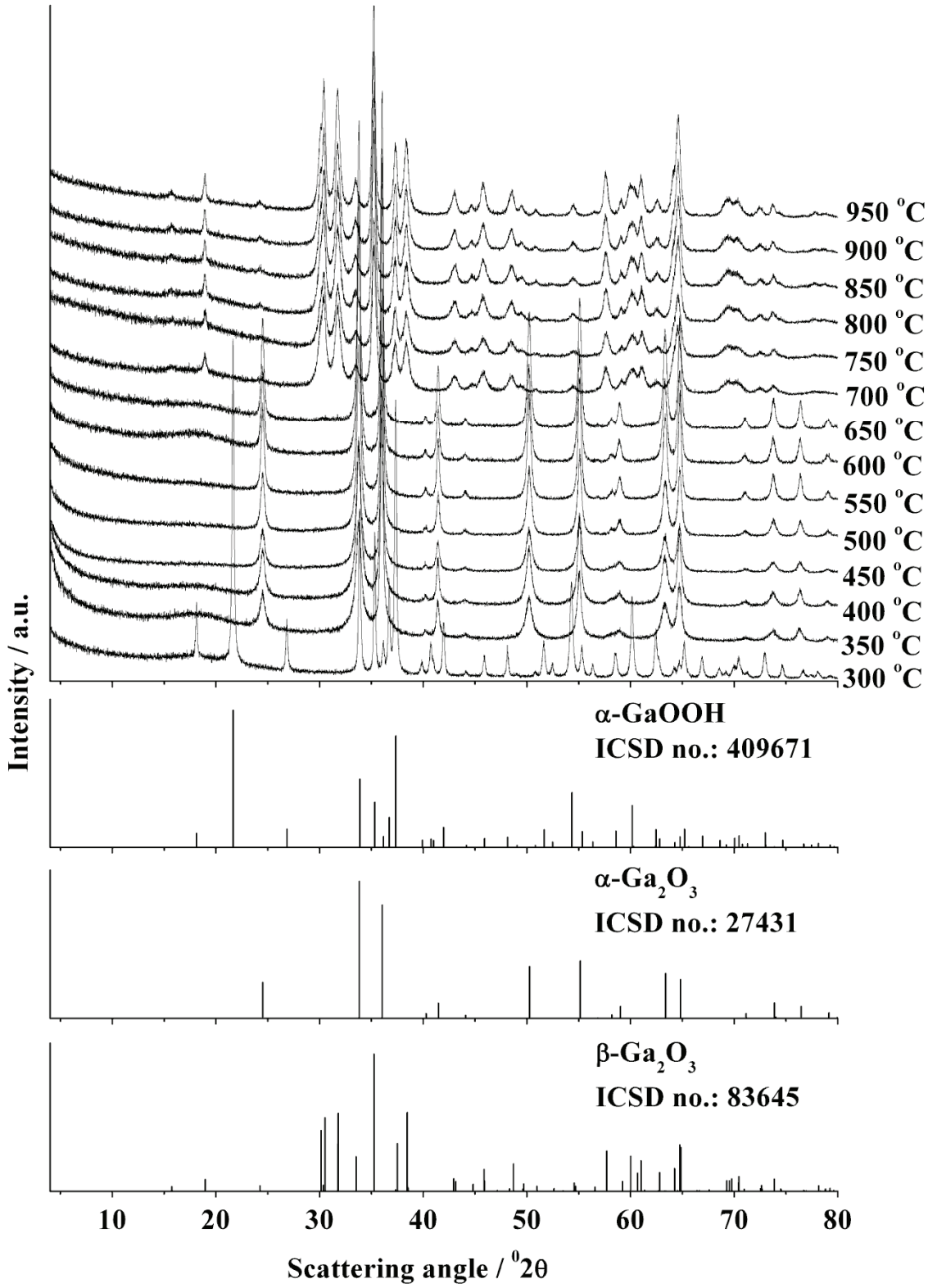
950 °C
900 °C
850 °C
800 °C
750 °C
700 °C
650 °C
600 °C
550 °C
500 °C
450 °C
400 °C
350 °C
300 °C
Intensity / a.u.
α-GaOOH
ICSD no.: 409671
α-Ga2O3
ICSD no.: 27431
β-Ga2O3
ICSD no.: 83645
10
20
30
40
50
60
70
80
Scattering angle / 02θ

Figure 6

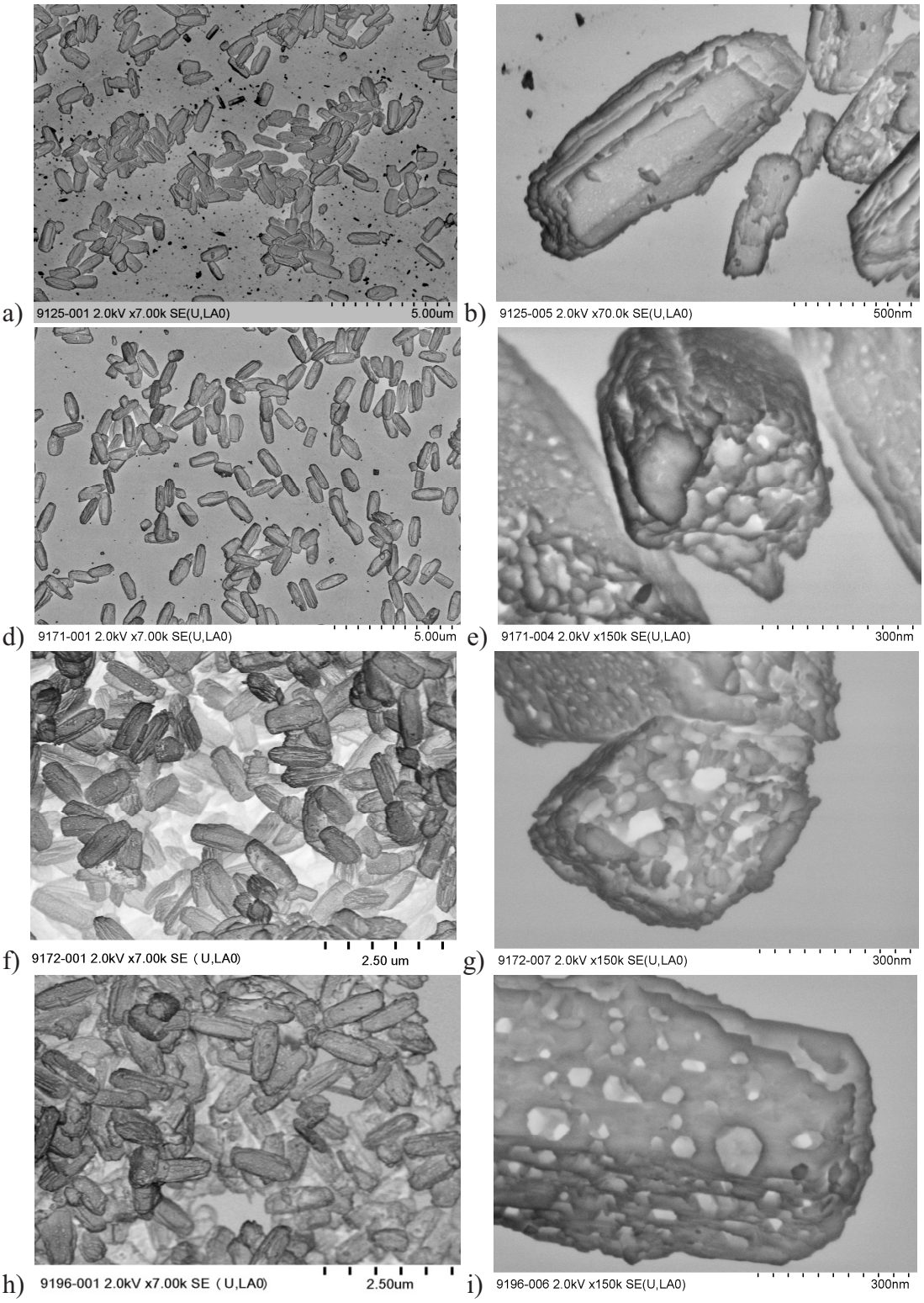
a)
9125-001 2.0kV x7.00k SE(U,LA0)
5.00um
b)
9125-005 2.0kV x70.0k SE(U,LA0)
500nm
d)
9171-001 2.0kV x7.00k SE(U,LA0)
5.00um
e)
9171-004 2.0kV x150k SE(U,LA0)
300nm
f)
9172-001 2.0kV x7.00k SE (U,LA0)
2.50 um
g)
9172-007 2.0kV x150k SE(U,LA0)
300nm
h)
9196-001 2.0kV x7.00k SE (U,LA0)
2.50um
i)
9196-006 2.0kV x150k SE(U,LA0)
300nm

Figure 7

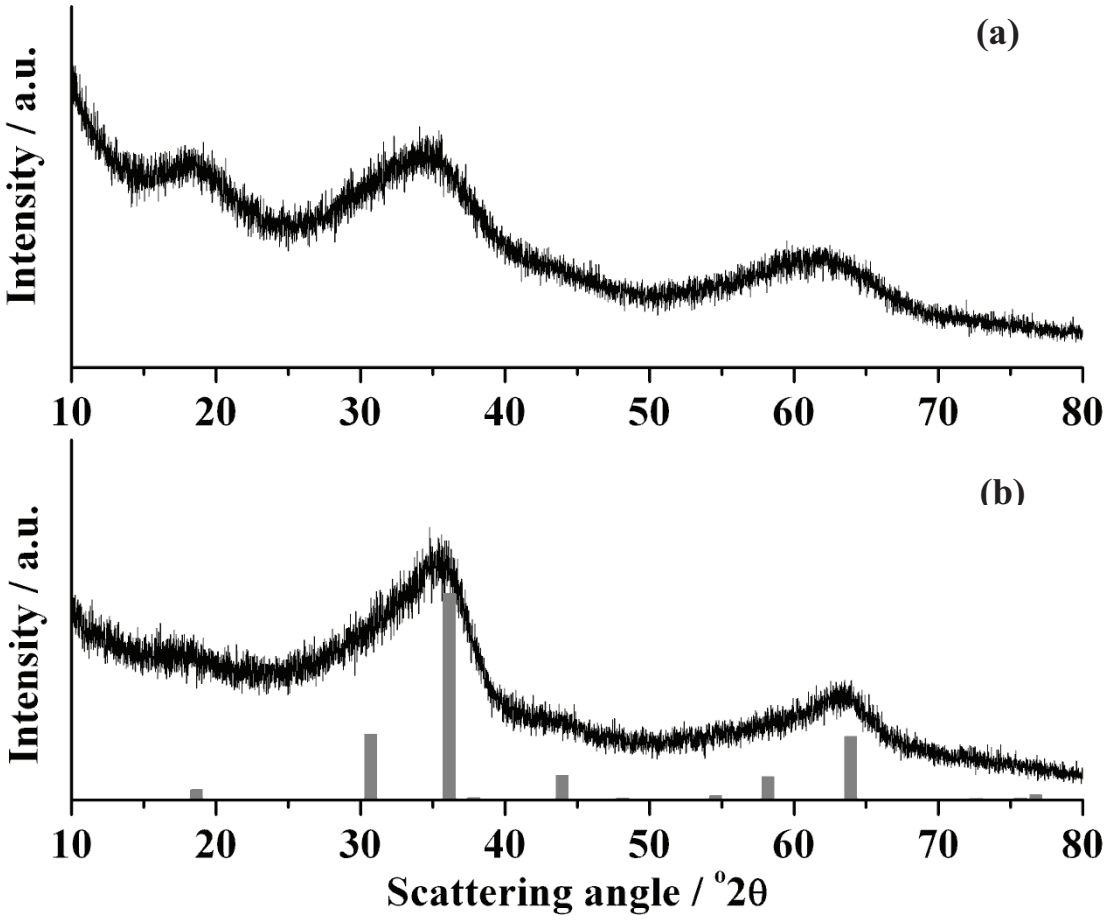
(a)
Intensity / a.u.
10
20
30
40
50
60
70
80
(b)
Intensity / a.u.
10
20
30
40
50
60
70
80
Scattering angle / °2θ

Figure 8

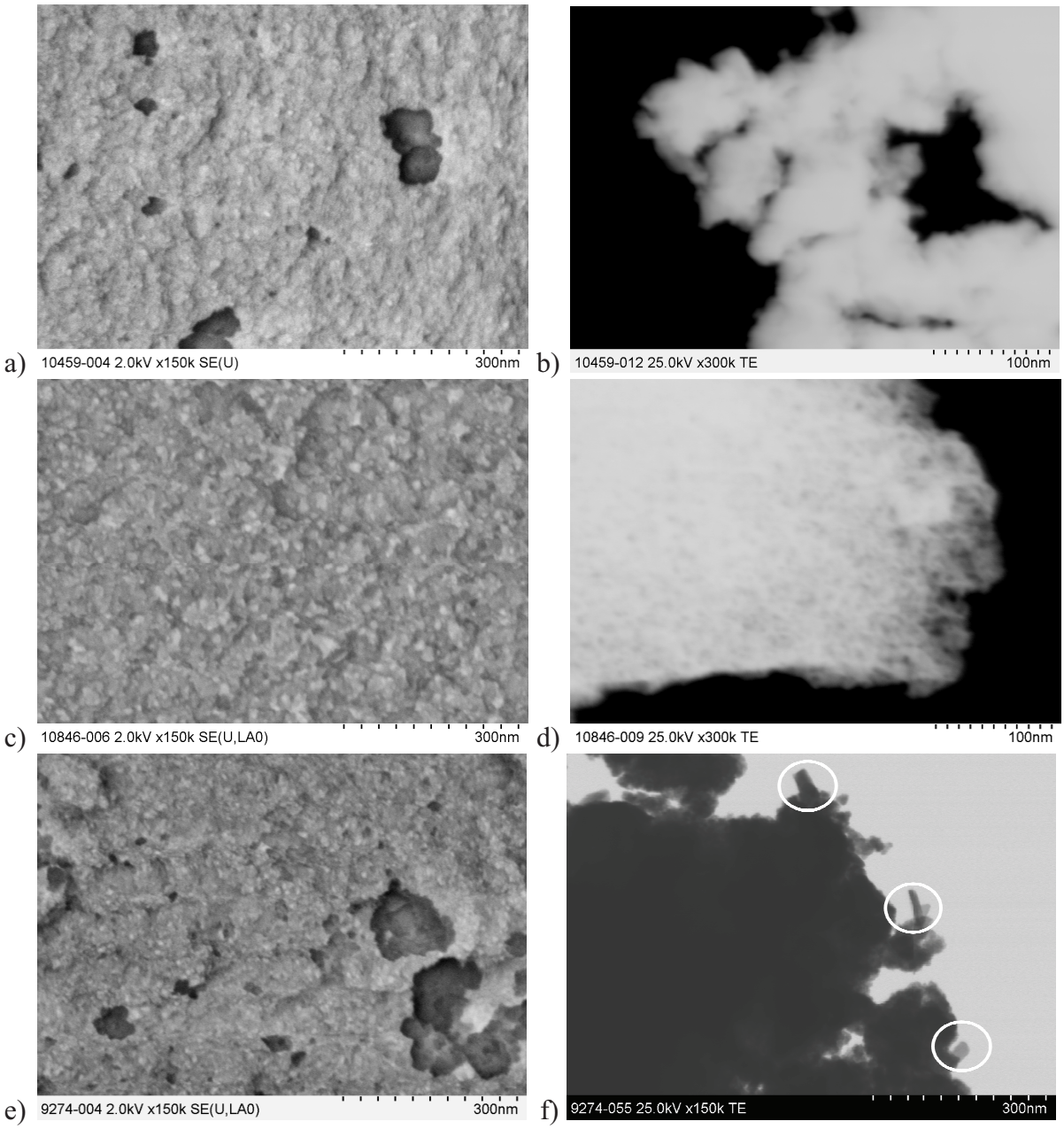
a)
10459-004 2.0kV x150k SE(U)
300nm
b)
10459-012 25.0kV x300k TE
100nm
c)
10846-006 2.0kV x150k SE(U,LA0)
300nm
d)
10846-009 25.0kV x300k TE
100nm
e)
9274-004 2.0kV x150k SE(U,LA0)
300nm
f)
9274-055 25.0kV x150k TE
300nm

Figure 9

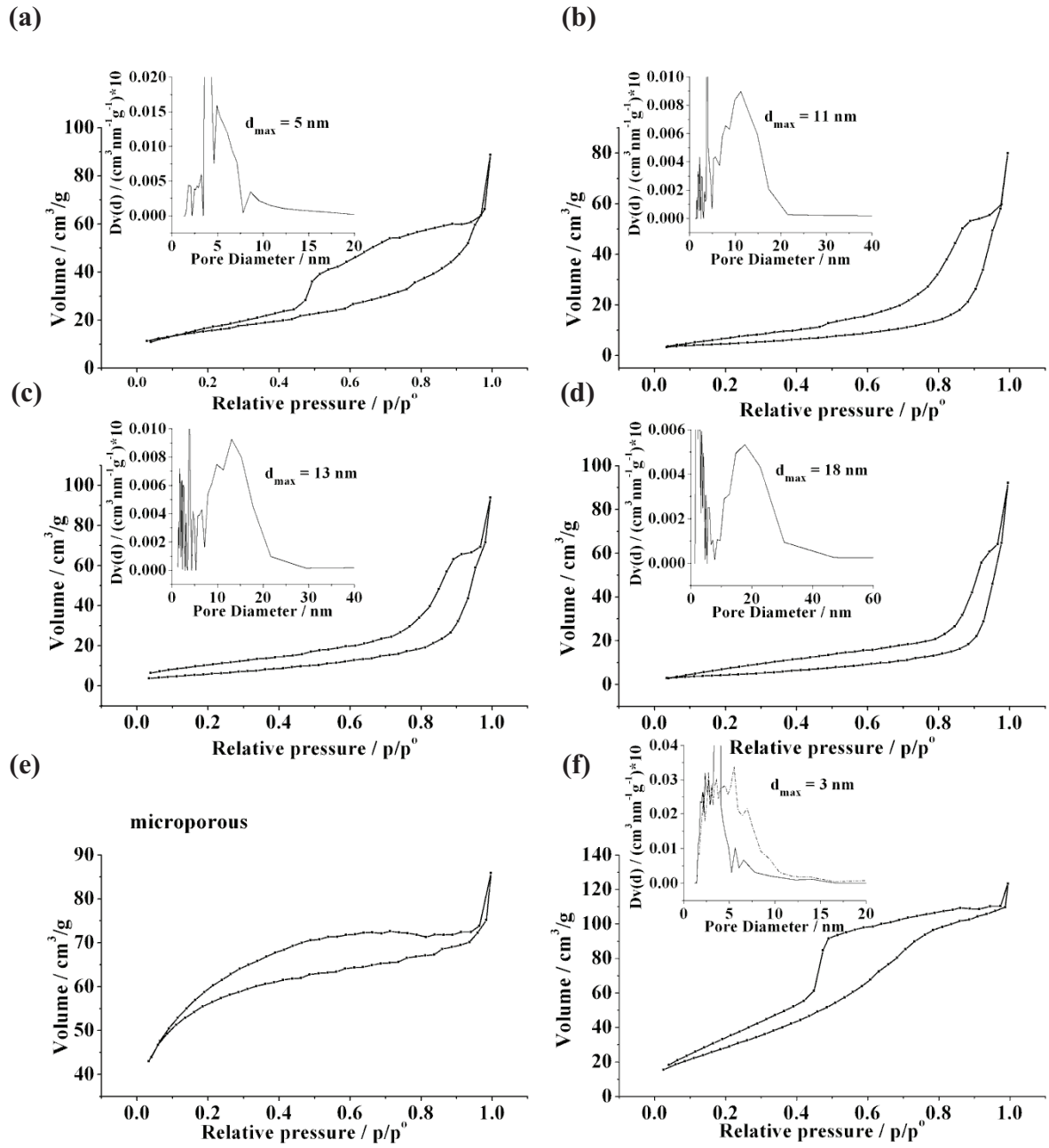
(a)
(b)
(c)
(d)
(e)
(f)
Volume / cm³/g
Relative pressure / p/p°
Dv(d) / (cm³ nm⁻¹ g⁻¹)*10
Pore Diameter / nm
d_max = 5 nm
d_max = 11 nm
d_max = 13 nm
d_max = 18 nm
d_max = 3 nm
microporous

Figure 10

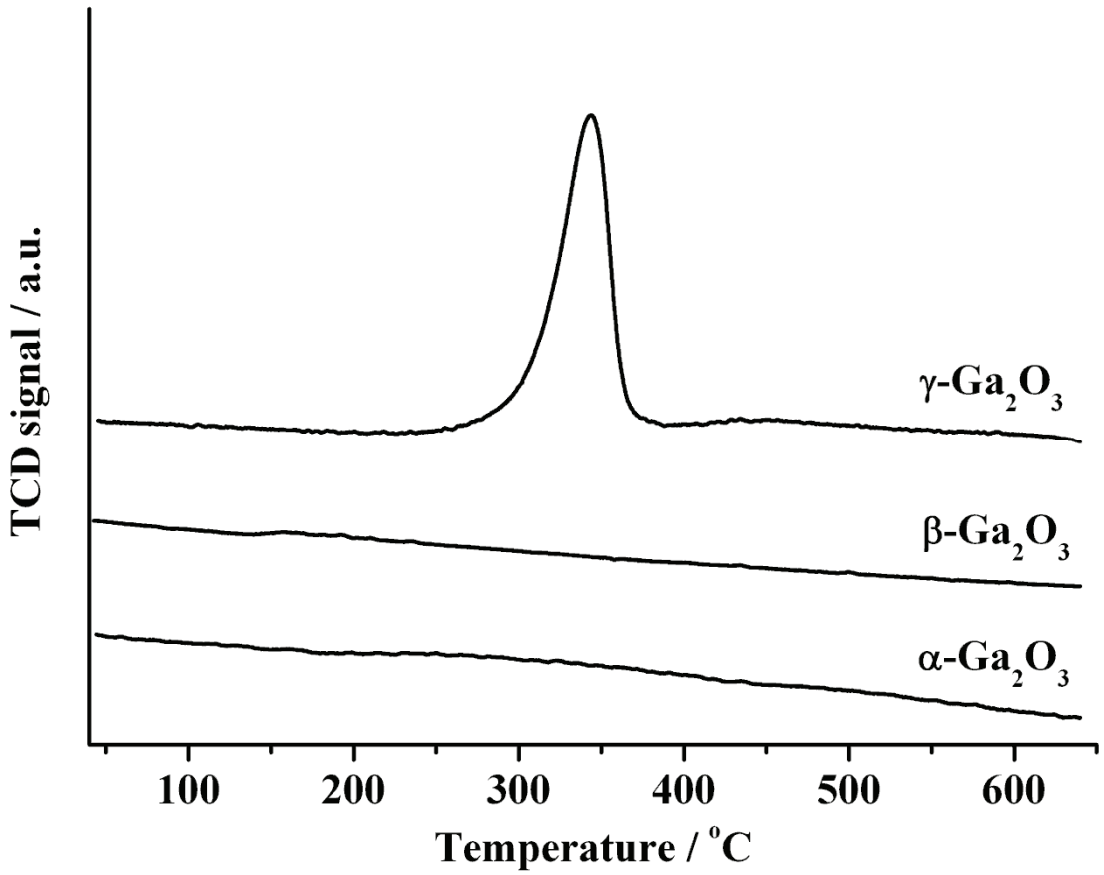
TCD signal / a.u.
γ-Ga2O3
β-Ga2O3
α-Ga2O3
100
200
300
400
500
600
Temperature / °C

Figure 11

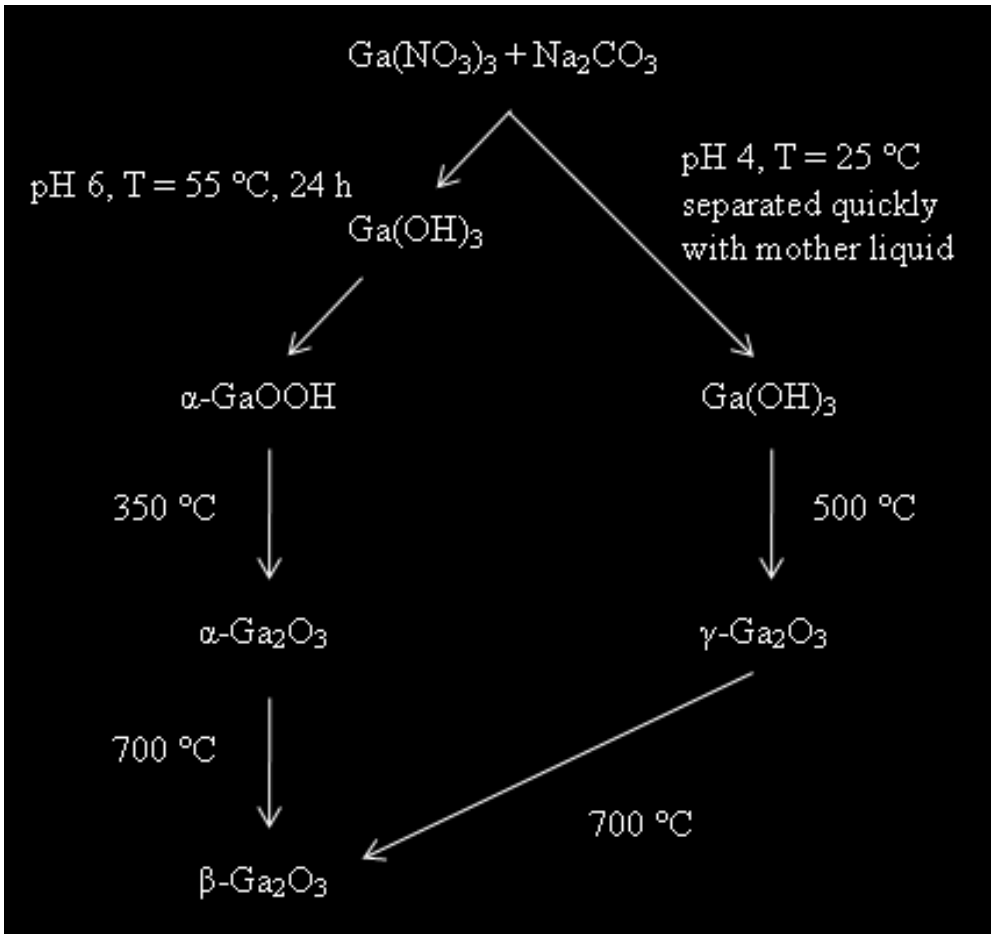
Ga(NO3)3 + Na2CO3
pH 6, T = 55 °C, 24 h
Ga(OH)3
pH 4, T = 25 °C
separated quickly
with mother liquid
α-GaOOH
Ga(OH)3
350 °C
500 °C
α-Ga2O3
γ-Ga2O3
700 °C
700 °C
β-Ga2O3

Figure 12